Publisher: GSA
Journal: GEOL: Geology
DOI:10.1130/G39672.1

Determining the 3-D geometry of a dike swarm and its impact on later rift geometry using seismic reflection data

Thomas B. Phillips*, Craig Magee, Christopher A-L. Jackson, and Rebecca E. Bell

Basins Research Group (BRG), Department of Earth Science and Engineering, Imperial College, Prince Consort Road, London SW7 2BP, UK

*E-mail: tp813@ic.ac.uk

ABSTRACT

Dike swarm emplacement accommodates extension during rifting and large igneous province (LIP) formation, whereas ancient dike swarms can localize strain during later tectonic events. Deciphering three-dimensional (3-D) dike swarm geometry is critical to accurately calculating magma volumes and magma-assisted crustal extension, allowing syn-emplacement mantle and tectonic processes to be interrogated, and for quantifying the influence ancient dike swarms have, post-emplacement, on faulting. However, the 2-D nature of Earth's surface, combined with the difficulties in imaging sub-vertical dikes on seismic reflection data, and the relatively low resolution of geophysical data in areas of active diking, means that our understanding of dike swarm geometry at depth is limited. We examine an ~25-km-wide, >100-km-long, west-southwest–trending dike swarm imaged, due to post-emplacement rotation to shallower dips, in high-quality 2-D and 3-D seismic reflection data offshore southern Norway. Tuned reflection packages correspond to thin (<75 m thick), closely-spaced dikes. These data provide a unique opportunity to image and map an ancient dike swarm at variable structural levels. Cross-cutting relationships indicate emplacement occurred in the Late

Carboniferous-Early Permian, and was linked to the formation of the ca. 300 Ma Skagerrak-centered LIP. Dike swarm width increases with depth, suggesting that magma volume and crustal extension calculations based on surface exposures are dependent on the level of erosion. During the Mesozoic, rift-related faults localized above and exploited mechanical anisotropies within the dike swarm. We demonstrate that seismic reflection data are a powerful tool in understanding dike swarm geometry and the control of dikes on subsequent faulting.

INTRODUCTION

Dike swarm emplacement facilitates magma transport over significant vertical and lateral distances (e.g., Ernst and Buchan, 1997; Torsvik et al., 2008) and accommodates extension, particularly during large igneous province (LIP) formation and magma-rich continental breakup (e.g., Kendall et al., 2005; Keir et al., 2006). Furthermore, following emplacement and solidification, dike swarms form mechanical anisotropies within the crust, serving to localize strain during later tectonic events (e.g., Dineva et al., 2007). Dike swarms thus influence the syn- and post-emplacement tectonic evolution of many regions, leading numerous studies to (1) use their plan-view geometry and distribution to calculate melt volumes and extension associated with rifting and LIP emplacement, and thus infer mantle and tectonic processes (e.g., Halls, 1982); and (2) further understand rift evolution through correlating their location and geometry to that of later-formed structures (e.g., Dineva et al., 2007). However, because the two-dimensional (2-D) nature of the Earth's surface only allows us to effectively investigate horizontal slices through dike swarms, we do not know whether dike swarm geometry varies with depth, or how, if at all, dike swarms influence the development of younger tectonic structures. Geophysical and geodetic data (e.g., interferometric synthetic aperture radar) capturing transient 'diking' events can provide insight into the 3-D geometry of individual dikes (e.g., Wright et al., 2006; White et al., 2011), but we typically rely on extrapolating surface or near-surface observations to depth to infer 3-D dike swarm structure (e.g., Kavanagh and Sparks, 2011).

Reflection seismology provides one of the only data sets that can constrain both the down-dip and along-strike geometry of dikes, as well as that of overlying structures, across broad areas (e.g., Malehmir and Bellefleur, 2010; Wall et al., 2010). While previous seismic-based studies have imaged or contain evidence of one or several dikes, which may or may not be part of a dike swarm (e.g., Zaleski et al., 1997; Malehmir and Bellefleur, 2010; Wall et al., 2010), we present, to the best of our knowledge, the first seismic data set that images and constrains the geometry of a dike swarm. We identify a 100-km-long, 25-km-wide, and 3-km-high section of a dike swarm in 2-D and 3-D seismic reflection data offshore southern Norway, which consists of numerous, closely spaced dikes that are imaged because the swarm has been rotated post-emplacement and now dips at ~50° (Fig. 1a). These data present a unique and exciting opportunity to examine dike swarm geometry with depth and quantitatively assess how the dike swarm influenced the development of a younger, overlying normal fault array.

GEOLOGICAL SETTING

The east-trending Farsund Basin is located just offshore southern Norway (Fig. 1a). The basin defines a south-dipping half-graben, with the southern margin delineated by the Carboniferous-Permian Fjerritslev fault system (Figs. 1b and 1c) (e.g., Mogensen and Jensen, 1994). Reactivation of this fault during Late Jurassic-to-Early Cretaceous

Publisher: GSA
Journal: GEOL: Geology
DOI:10.1130/G39672.1

extension caused flexure in its hanging wall (Fig. 1c) (Mogensen and Jensen, 1994). Nearby wells (Fig. 1a) penetrate down to Lower-Middle Permian strata, which likely overlies Permian-Carboniferous strata. We interpret the deepest horizon that can confidently be mapped within our seismic data as the ca. 290–270 Ma Saalian-Altmark unconformity (Figs. 1b and 2a) (Glennie, 1997).

DATASET AND METHODOLOGY

Our main data set is a pre-stack time-migrated, 2-D seismic reflection data set consisting of <5-km-spaced, north-trending seismic sections with a total line length of 2158 km. We also use several other time-migrated 2-D data sets, and a time-migrated, ~500 km^2 3-D data set in the west of the study area (Fig. DR1 in the GSA Data Repository[1]). The 2-D data image to at least 7 s two-way time (TWT) (~15 km), and the 3-D volume to 4 s TWT (~7 km). Seismic horizon age is constrained by boreholes, the deepest of which terminates in basement below Permian strata (Well 11/5–1; Fig. 1a); no boreholes penetrate the interpreted dike swarm. We performed quantitative analyses, in the form of throw-depth plots (see the Data Repository), on a number of stratigraphically younger faults that are spatially correlated to the underlying dike swarm.

DIKE SWARM SEISMIC CHARACTER

We observe a series of inclined (apparent dips of ~35–50°N), north-dipping, high-amplitude reflections along the northern margin of the Farsund Basin within an ~25-km-wide by ~100-km-long, west-southwest–trending zone (Figs. 1 and 2). Inclined reflections in the swarm center are truncated by the overlying Saalian-Altmark and Base Zechstein unconformities (Fig. 2). These reflections are confidently interpreted between ~0.8–2.5 s TWT (~1–4 km), below which image quality deteriorates, although they appear to continue to greater depths (Figs. 1c and 2). To the west and south, the inclined reflections are deeper (>2.5 s TWT) and relatively poorly imaged (Fig. 1c); mapping of the reflections further east is not possible due to a lack of data. The density of inclined reflections changes across the width of the zone, from ~10 reflection peaks/km in the center, to ~6 peaks/km at the margins (Fig. 2a). The upper tips of many of the reflections at the margins terminate at stratigraphically lower levels than those in the center (Figs. 1b and 2a); the width of the reflection package thus increases with depth, from ~12 km at the Saalian-Altmark unconformity down to ~20 km where image quality deteriorates.

The inclined reflections may represent a number of different features, including geophysical processing-related artifacts, tilted sedimentary strata, fault-plane reflections, or dikes. We dismiss the first three hypotheses because the inclined reflections (1) are imaged within several 2-D and 3-D seismic surveys, which have different acquisition and processing parameters (see Table DR1 in the Data Repository), implying they are not geophysical (e.g., processing or acquisition) artifacts; (2) do not resemble reflections overlying in the cover, or adjacent inclined reflections (Fig. 2a), suggesting they are not seismic multiples; (3) cross-cut south-dipping (~10–20°S) reflections associated with Carboniferous-Permian strata, implying they themselves do not represent sedimentary layers (Fig. 2a); and (4) rarely offset the Carboniferous-Permian stratigraphic reflections, indicating that most do not represent fault-plane reflections (Fig. 2). As a result, we favor the interpretation that the majority of the inclined reflections represent dikes, and refer to the overall package as the ‘Farsund Dike Swarm.’ As the dike swarm cross-cuts probable Carboniferous-Permian (<320 Ma) strata and is itself truncated by the 290–270 Ma

Saalian-Altmark unconformity (Fig. 2a), we infer an emplacement age of ca. 320–270 Ma.

Having established the inclined reflections likely represent dikes, we compare our observations of dike swarm geometry across an extensive depth range (~1–3 km), to field- and modeling-based studies reliant on 2-D plan-view exposures (Kavanagh and Sparks, 2011; Bunger et al., 2013). The vertical resolution (i.e., $\lambda/4$, where λ is the seismic wavelength) of the seismic data dictates the maximum (i.e., vertical) thickness of individual dikes for which both margins can be fully resolved, while the thinnest detectable dikes will typically have a vertical thickness of $\lambda/30$ (Slatt, 2006); these parameters can be calculated from the seismic frequency (~20 Hz) and velocity of the interval of interest. Because we have no well data to constrain the seismic velocity of the dike rocks and do not know the ratio of igneous to sedimentary material, we use a range of seismic velocities from 6 km/s (i.e., purely igneous material; Smallwood and Maresh, 2002) to 3 km/s (i.e., negligible igneous material) to conduct our depth conversion. These velocities imply that the dike dip is between 35 and 50°. We calculate vertical resolutions of 37.5–75 m and detection limits of 5–10 m. The Farsund Dike Swarm is composed of tuned reflection packages, indicating multiple, relatively thin (<75 m), and closely spaced dikes. We cannot determine whether each package represents interference between reflections arising from the margins of one or several dikes; as a result, we cannot assess detailed dike spacing or thickness. The lateral distance between inclined reflections, perhaps a proxy for dike spacing, does, however, appear to increase toward the margins, where the majority of dikes terminate at deeper stratigraphic levels than those in the swarm center (Fig. 2a). This inverse relationship is inconsistent with analytical model predictions, which suggest spacing increases with dike height (cf. Bunger et al., 2013), it is plausible that dike swarm emplacement was relatively protracted, with younger dikes preferentially intruded into the center of the swarm, thereby reducing spacing.

The observation that dike height varies across the swarm (Fig. 2) further indicates that dikes exposed in plan-view at the Earth's surface may not represent true dike swarm width, and could significantly influence magma volume and associated extension calculations. For example, assuming a 1:1 dike to host rock ratio, a swarm length of 50 km, and a dike height of 3 km, dike swarm volumes calculated from the measured widths at the Saalian-Altmark unconformity (i.e., 12 km) and a deeper level (e.g., 20 km) would be 900 km^3 and 1500 km^3, respectively, with associated extension measurements of 6 and 10 km respectively.

TECTONO-MAGMATIC CONTEXT AND SIGNIFICANCE OF THE FARSUND DIKE SWARM

The west-southwest–trending, Late-Carboniferous-to-Early Permian (emplaced between 320 and 270 Ma) Farsund Dike Swarm is contemporaneous with a 300–280 Ma phase of dike emplacement and volcanic activity across Central and Northern Europe (see Torsvik et al., 2008, and references therein). Paleogeographic reconstructions indicate that onshore dikes intruded during this magmatic event are distributed radially about the Skagerrak-centered LIP (ScLIP; Fig. 3) (Torsvik et al., 2008). We suggest that the Farsund Dike Swarm links to the Midland Valley Dike Suite in the United Kingdom, forming a proximal part to a >1000-km-long, western arm of a trilete radial dike swarm laterally injected from the ScLIP (Fig. 3).

DIKE-FAULT INTERACTIONS

A series of north-dipping, Mesozoic faults overlie and link with the Farsund Dike Swarm (Figs. 1b and 2). Kinematic analysis (see supplementary information) identifying the site of maximum throw indicates these faults nucleated at or just above the top of the dike swarm (Fig. 2d). Large negative throw gradients present around the Top Jurassic possibly indicate erosion at this time, being overlain by a low-throw segment that is indicative of fault reactivation (Fig. 2d) (e.g., Cartwright et al., 1998). The faults likely initiated in the Triassic in response to margin flexure; reactivation occurred due to slip on and associated hanging wall flexure of the Fjerritslev Fault during Late Jurassic-Early Cretaceous extension (Fig. 4) (Mogensen and Jensen, 1994). This flexure rotated the Farsund Dike Swarm, allowing it to be imaged in seismic data (Fig. 4). Overall, weaknesses within the dike swarm (e.g., dike contacts) localized rift-related strain and were exploited by these later formed faults.

CONCLUSIONS

We present images of one of the first dike swarms to be imaged in seismic reflection data. The swarm trends west-southwest, is 25 km wide, and is constrained to at least ~3 km depth. Seismic-stratigraphic and geometric constraints link the swarm to the ca. 300 Ma ScLIP, and show that it forms, along with the Midland Valley Dyke Suite, part of an ~1000-km-long system across the North Sea. Post-emplacement, regional faulting rotated the swarm to ~50° dip, allowing its imaging on seismic reflection data. By imaging the dike swarm in cross-section, we highlight a variable dike swarm width with depth. This observation is not possible based on plan-view sections at the Earth’s surface alone and shows how calculations of crustal extension and magma volumes may be dependent on the level of erosion of the dike swarm. We show that normal faults later exploited internal mechanical anisotropies between individual dikes. Our imaging of a dike swarm at depth offers new insights into their geometry, and implications for their role in continental extension, in addition to showcasing how dike swarms can influence tectonic events after their emplacement.

ACKNOWLEDGMENTS

We thank Petroleum Geo-Services (PGS) for allowing us to show the seismic data in this study, along with Schlumberger Ltd. for providing academic licenses for the Petrel software. This contribution forms part of the MultiRift Project funded by the Research Council of Norway's PETROMAKS program (Project number 215591) and Statoil. We thank S. Holford, A. Malehmir, an anonymous reviewer, and editor D. Brown, for their constructive comments, along with members of the Basins Research Group.

REFERENCES CITED

Bunger, A.P., Menand, T., Cruden, A., Zhang, X., and Halls, H., 2013, Analytical predictions for a natural spacing within dyke swarms: Earth and Planetary Science Letters, v. 375, p. 270–279, https://doi.org/10.1016/j.epsl.2013.05.044.

Cartwright, J., Bouroullec, R., James, D., and Johnson, H., 1998, Polycyclic motion history of some Gulf Coast growth faults from high-resolution displacement analysis: Geology, v. 26, p. 819–822, https://doi.org/10.1130/0091-7613(1998)026<0819:PMHOSG>2.3.CO;2.

Dineva, S., Eaton, D., Ma, S., and Mereu, R., 2007, The October 2005 Georgian Bay, Canada, earthquake sequence: Mafic dykes and their role in the mechanical heterogeneity of Precambrian crust: Bulletin of the Seismological Society of America, v. 97, p. 457–473, https://doi.org/10.1785/0120060176.

Ernst, R.E., and Buchan, K.L., 1997, Giant radiating dyke swarms: Their use in identifying pre-Mesozoic large igneous provinces and mantle plumes, *in* Mahoney, J.J., and Coffin, M.F., eds., Large Igneous Provinces. Continental, Oceanic, and Planetary Flood Volcanism: Washington, D.C., American Geophysical Union Monograph 100, p. 297–333, https://doi.org/10.1029/GM100p0297.

Glennie, K.W., 1997, Recent advances in understanding the southern North Sea Basin: A summary: Geological Society of London Special Publications, v. 123, p. 17–29, https://doi.org/10.1144/GSL.SP.1997.123.01.03.

Halls, H., 1982, The importance and potential of mafic dyke swarms in studies of geodynamic processes: Geoscience Canada, v. 9, p. 145–154.

Heeremans, M., Faleide, J.I., and Larsen, B.T., 2004, Late Carboniferous -Permian of NW Europe: An introduction to a new regional map: Geological Society of London Special Publications, v. 223, p. 75–88, https://doi.org/10.1144/GSL.SP.2004.223.01.04.

Kavanagh, J., and Sparks, R.S.J., 2011, Insights of dyke emplacement mechanics from detailed 3D dyke thickness datasets: Journal of the Geological Society, v. 168, p. 965–978, https://doi.org/10.1144/0016-76492010-137.

Keir, D., Ebinger, C.J., Stuart, G.W., Daly, E., and Ayele, A., 2006, Strain accommodation by magmatism and faulting as rifting proceeds to breakup: Seismicity of the northern Ethiopian rift: Journal of Geophysical Research: Solid Earth, v. 111, http://doi.org/10.1029/2005JB003748

Kendall, J.M., Stuart, G.W., Ebinger, C.J., Bastow, I.D., and Keir, D., 2005, Magma-assisted rifting in Ethiopia: Nature, v. 433, p. 146–148, https://doi.org/10.1038/nature03161.

Magee, C., McDermott, K.G., Stevenson, C.T.E., and Jackson, C.A.L., 2014, Influence of crystallised igneous intrusions on fault nucleation and reactivation during continental extension: Journal of Structural Geology, v. 62, p. 183–193, https://doi.org/10.1016/j.jsg.2014.02.003.

Malehmir, A., and Bellefleur, G., 2010, Reflection seismic imaging and physical properties of base-metal and associated iron deposits in the Bathurst Mining Camp, New Brunswick, Canada: Ore Geology Reviews, v. 38, p. 319–333, https://doi.org/10.1016/j.oregeorev.2010.08.002.

Mogensen, T.E., and Jensen, L.N., 1994, Cretaceous subsidence and inversion along the Tornquist Zone from Kattegat to the Egersund Basin: First Break, v. 12, p. 211–222, https://doi.org/10.3997/1365-2397.1994016.

Slatt, R.M., 2006, Stratigraphic Reservoir Characterization for Petroleum Geologists, Geophysicists, and Engineers: Amsterdam, Elsevier, 688 p.

Smallwood, J.R., and Maresh, J., 2002, The properties, morphology and distribution of igneous sills: modelling, borehole data and 3D seismic from the Faroe-Shetland area: Geological Society of London, Special Publications, v. 197, p. 271–306, https://doi.org/10.1144/GSL.SP.2002.197.01.11.

Torsvik, T.H., Smethurst, M.A., Burke, K., and Steinberger, B., 2008, Long term stability in deep mantle structure: Evidence from the~ 300 Ma Skagerrak-Centered Large

Igneous Province (the SCLIP): Earth and Planetary Science Letters, v. 267, p. 444–452, https://doi.org/10.1016/j.epsl.2007.12.004.

Wall, M., Cartwright, J., Davies, R., and McGrandle, A., 2010, 3D seismic imaging of a tertiary dyke swarm in the southern North Sea, UK: Basin Research, v. 22, p. 181–194, https://doi.org/10.1111/j.1365-2117.2009.00416.x.

White, R.S., Drew, J., Martens, H.R., Key, J., Soosalu, H., and Jakobsdóttir, S.S., 2011, Dynamics of dyke intrusion in the mid-crust of Iceland: Earth and Planetary Science Letters, v. 304, p. 300–312, https://doi.org/10.1016/j.epsl.2011.02.038.

Wright, T.J., Ebinger, C., Biggs, J., Ayele, A., Yirgu, G., Keir, D., and Stork, A., 2006, Magma-maintained rift segmentation at continental rupture in the 2005 Afar dyking episode: Nature, v. 442, p. 291–294, https://doi.org/10.1038/nature04978.

Zaleski, E., Eaton, D.W., Milkereit, B., Roberts, B., Salisbury, M., and Petrie, L., 1997, Seismic reflections from subvertical diabase dikes in an Archean terrane: Geology, v. 25, p. 707–710, https://doi.org/10.1130/0091-7613(1997)025<0707:SRFSDD>2.3.CO;2.

FIGURE CAPTIONS

Figure 1. A: Two-way travel time structure map of the Base Zechstein (Upper Permian) surface showing the extent of the Farsund Dike Swarm. Areas of high and low confidence interpretation are shown in dark gray and light gray, respectively, based upon the clarity of the steeply inclined reflections. B: Stratigraphic column detailing mapped horizons and regional tectonics. C: Interpreted regional seismic section. Some dikes are highlighted in green, although the majority are uninterpreted. Seismic data are shown

DOI:10.1130/G39672.1

using the Society of Exploration Geophysicists reverse polarity convention. See the Data Repository (see footnote 1) for uninterpreted section.

Figure 2. A: Interpreted seismic section showing dike swarm seismic character, and stratigraphic and fault relationships. B, C: Seismic sections showing dike seismic character within interpreted swarm. D: Throw-length profiles for the faults highlighted in Figures 1A and 2A. See Figure 1A for figure locations. See the Data Repository (see footnote 1) for uninterpreted sections.

Figure 3. Location of the Farsund Dike Swarm in relation to the regional Skagerrak-centered LIP. Dikes and volcanic outlines follow Heeremans et al. (2004). Ages from Torsvik et al. (2008), and references therein).

Figure 4. Schematic evolution of the dike swarm. Dike emplacement occurs during the Permian-Carboniferous, before Early Cretaceous fault activity to the south causes rotation of the hanging wall, allowing imaging of the dike swarm and associated flexural faulting.

[1]GSA Data Repository item 2018xxx, xxxxxxxx, is available online at http://www.geosociety.org/datarepository/2018/ or on request from editing@geosociety.org.

Appendix A – Throw-depth analyses

T-z profiles can elucidate the kinematic history of normal faults (i.e. fault nucleation, growth, and/or reactivation) and thereby the tectonic evolution of sedimentary basins (see Mansfield and Cartwright, 1996; Cartwright et al., 1998 for a full description of the methods used). To assess how the Farsund Dike Swarm may have influenced the post-emplacement evolution of the study area, we calculated throw-depth (T-z) profiles along a number of key faults. We measure the hanging wall and footwall cut-offs of multiple stratigraphic horizons along the faults, plotting the calculated throw at the mid-point between the cut-offs. To accurately constrain the evolution of a fault, all fault slip-related strain must be explicitly recorded; i.e. we must incorporate both ductile (e.g. folding) and brittle (e.g. faulting) components of the strain field associated with fault slip (e.g. Meyer et al., 2002; Long and Imber, 2010; Whipp et al., 2014; Duffy et al., 2015; Jackson et al., 2017). Where fault-parallel folding occurs, hanging wall and footwall cut-offs were defined by projecting the regional dip of the horizon of interest, as measured some distance away from the fault, onto the fault plane.

Cartwright, J., Bouroullec, R., James, D., and Johnson, H., 1998, Polycyclic motion history of some Gulf Coast growth faults from high-resolution displacement analysis: Geology, v. 26, no. 9, p. 819-822.

Duffy, O. B., Bell, R. E., Jackson, C. A. L., Gawthorpe, R. L., and Whipp, P. S., 2015, Fault growth and interactions in a multiphase rift fault network: Horda Platform, Norwegian North Sea: Journal of Structural Geology, v. 80, p. 99-119.

Jackson, C. A.-L., Bell, R. E., Rotevatn, A., and Tvedt, A. B. M., 2017, Techniques to determine the kinematics of synsedimentary normal faults and implications for fault growth models: Geological Society, London, Special Publications, v. 439.

Long, J. J., and Imber, J., 2010, Geometrically coherent continuous deformation in the volume surrounding a seismically imaged normal fault-array: Journal of Structural Geology, v. 32, no. 2, p. 222-234.

Mansfield, C. S., and Cartwright, J. A., 1996, High resolution fault displacement mapping from three-dimensional seismic data: evidence for dip linkage during fault growth: Journal of Structural Geology, v. 18, no. 2–3, p. 249-263.

Meyer, V., Nicol, A., Childs, C., Walsh, J. J., and Watterson, J., 2002, Progressive localisation of strain during the evolution of a normal fault population: Journal of Structural Geology, v. 24, no. 8, p. 1215-1231.

Whipp, P. S., Jackson, C. A. L., Gawthorpe, R. L., Dreyer, T., and Quinn, D., 2014, Normal fault array evolution above a reactivated rift fabric; a subsurface example from the northern Horda Platform, Norwegian North Sea: Basin Research, v. 26, no. 4, p. 523-549.

Figure 1.

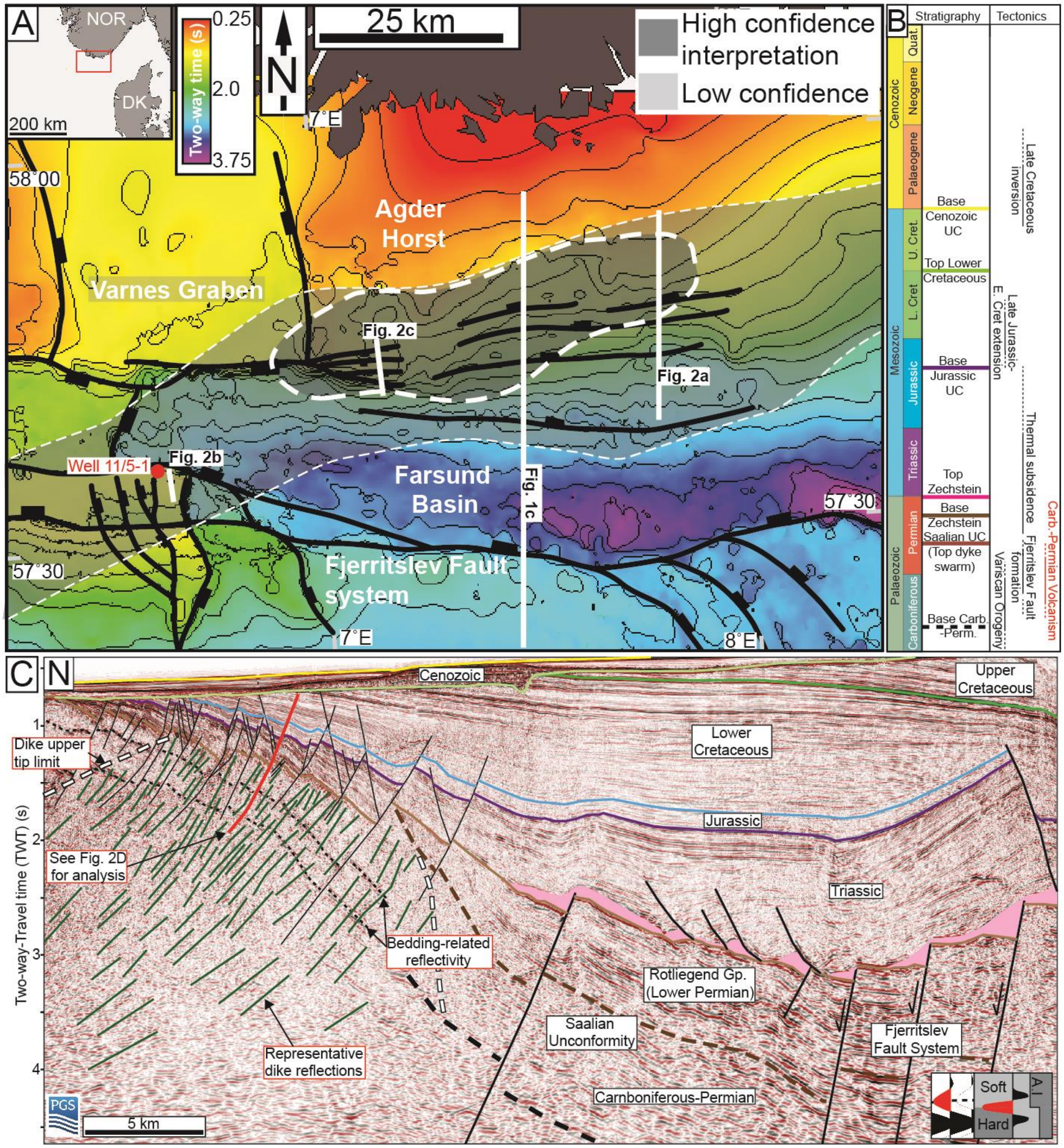
A
NOR
DK
200 km
Two-way time (s)
0.25
2.0
3.75
N
25 km
High confidence interpretation
Low confidence
7°E
58°00
Agder Horst
Varnes Graben
Fig. 2c
Fig. 2a
Well 11/5-1
Fig. 2b
Farsund Basin
Fig. 1c
57°30
Fjerritslev Fault system
8°E
B
Stratigraphy
Tectonics
Cenozoic
Quat.
Neogene
Palaeogene
Mesozoic
U. Cret.
L. Cret.
Jurassic
Triassic
Palaeozoic
Permian
Carboniferous
Base Cenozoic UC
Top Lower Cretaceous
Base Jurassic UC
Top Zechstein
Base Zechstein
Saalian UC
(Top dyke swarm)
Base Carb.-Perm.
Late Cretaceous inversion
Late Jurassic-E. Cret extension
Thermal subsidence
Fjerritslev Fault formation
Variscan Orogeny
Carb.-Permian Volcanism
C
N
Cenozoic
Upper Cretaceous
Lower Cretaceous
Jurassic
Triassic
Dike upper tip limit
See Fig. 2D for analysis
Bedding-related reflectivity
Rotliegend Gp. (Lower Permian)
Saalian Unconformity
Fjerritslev Fault System
Representative dike reflections
Carnboniferous-Permian
Two-way-Travel time (TWT) (s)
1
2
3
4
PGS
5 km
Soft
Hard
A.I.

Figure 2.

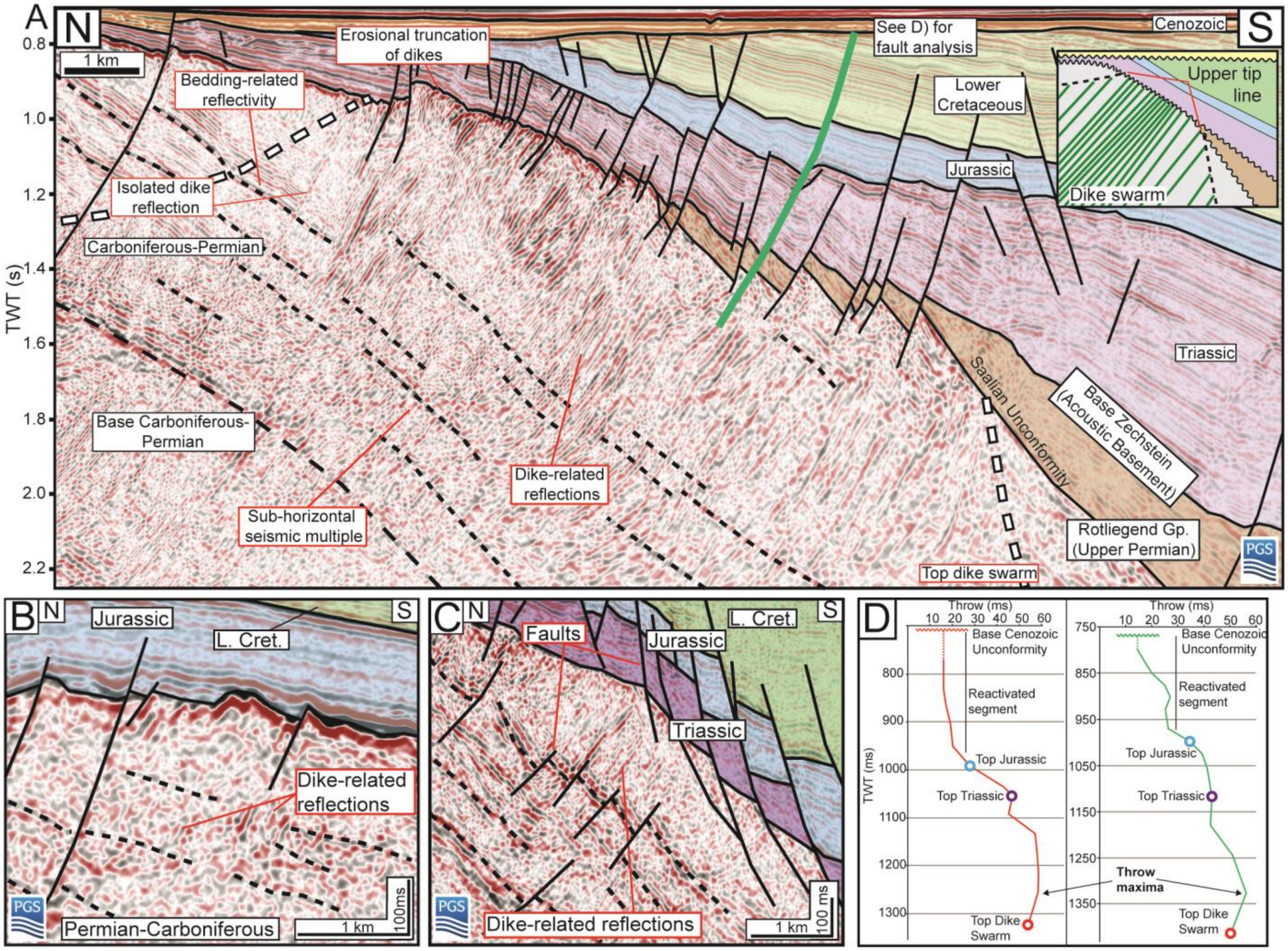
A
N
S
1 km
Erosional truncation of dikes
Bedding-related reflectivity
See D) for fault analysis
Cenozoic
Upper tip line
Lower Cretaceous
Jurassic
Dike swarm
Isolated dike reflection
Carboniferous-Permian
TWT (s)
0.8
1.0
1.2
1.4
1.6
1.8
2.0
2.2
Triassic
Saalian Unconformity
Base Zechstein (Acoustic Basement)
Base Carboniferous-Permian
Dike-related reflections
Sub-horizontal seismic multiple
Rotliegend Gp. (Upper Permian)
Top dike swarm
PGS
B
Jurassic
L. Cret.
Dike-related reflections
Permian-Carboniferous
100ms
C
Faults
Triassic
Dike-related reflections
100 ms
D
Throw (ms)
10 20 30 40 50 60
Base Cenozoic Unconformity
Reactivated segment
Top Jurassic
Top Triassic
Throw maxima
Top Dike Swarm
TWT (ms)
800
900
1000
1100
1200
1300
750
850
950
1050
1150
1250
1350

Publisher: GSA
Journal: GEOL: Geology
DOI:10.1130/G39672.1

Figure 3.

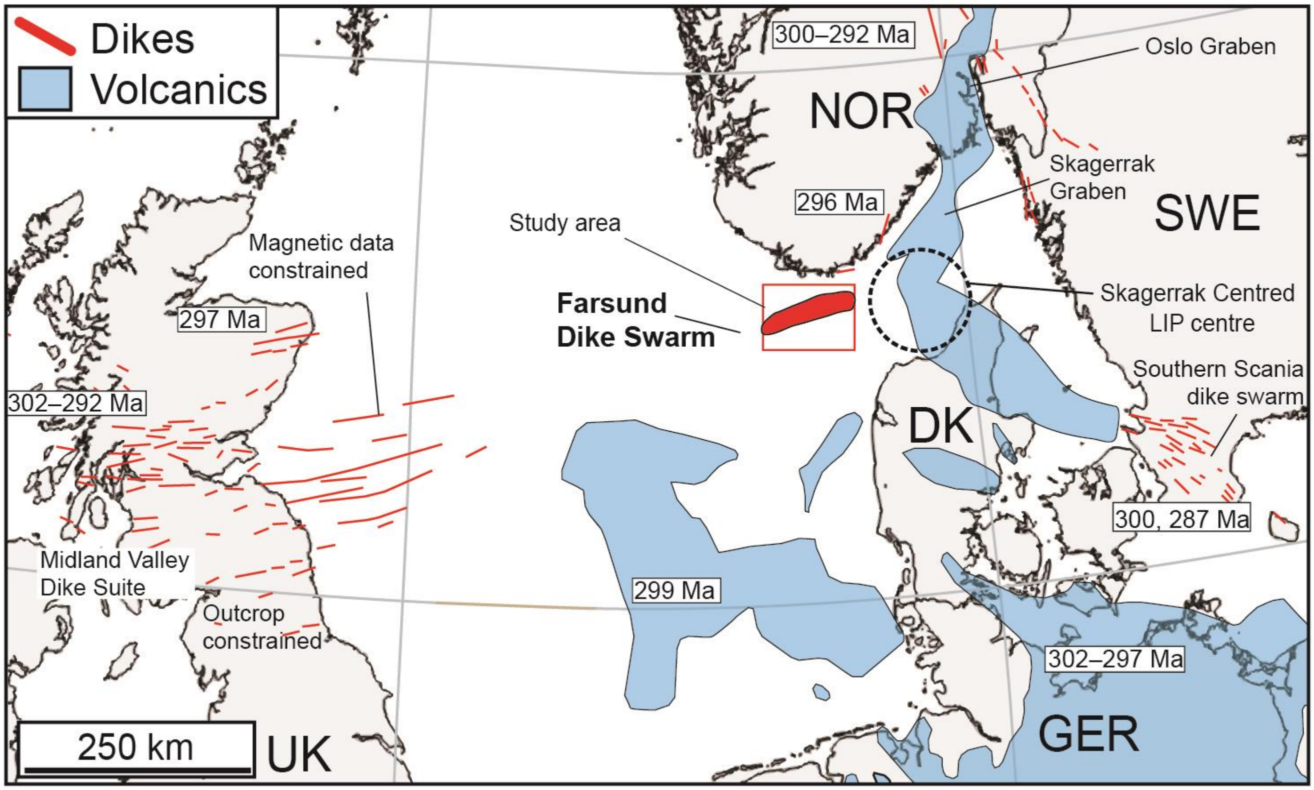

Publisher: GSA
Journal: GEOL: Geology
DOI:10.1130/G39672.1

342 Figure 4.

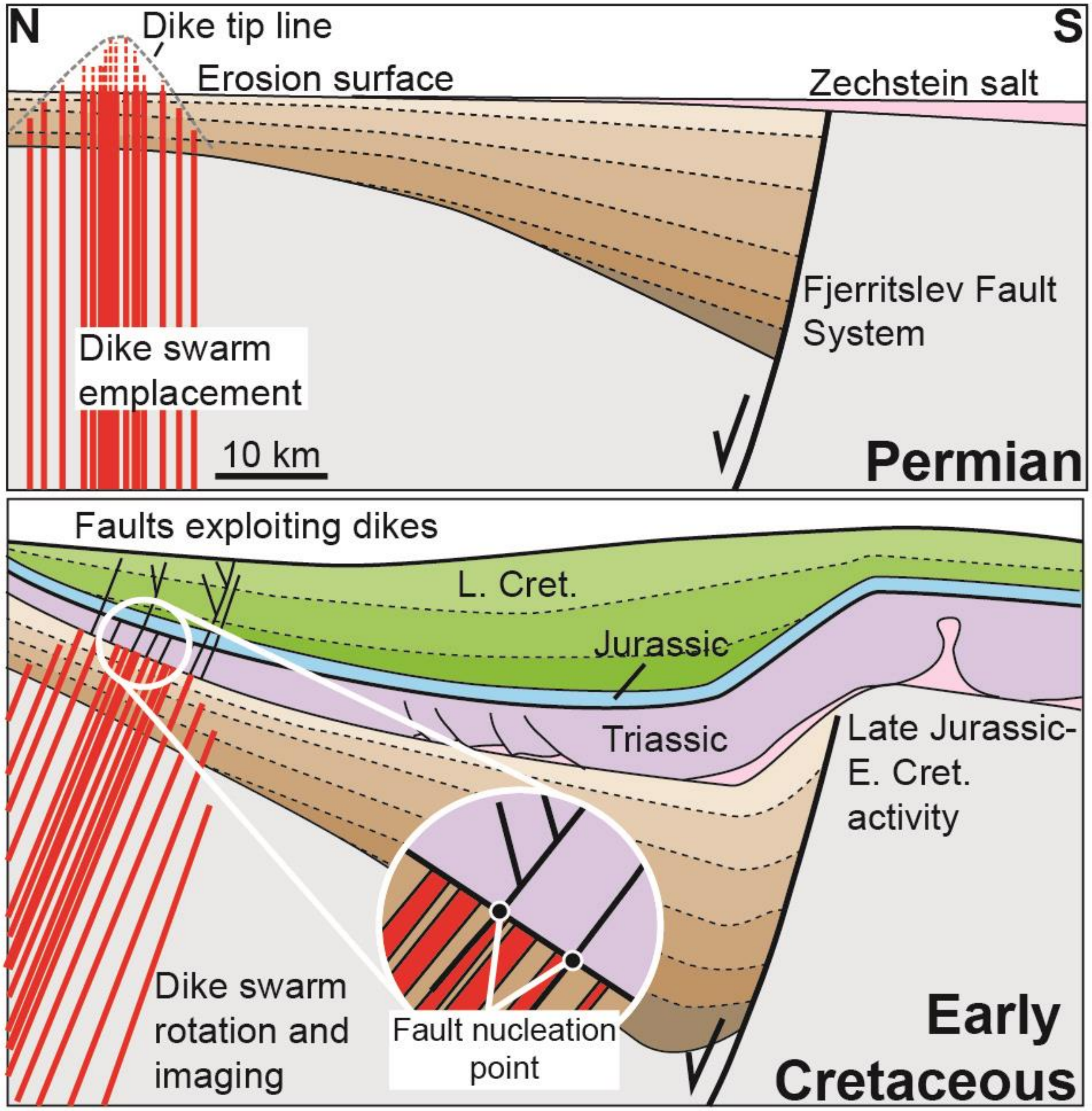

343
344
345

Publisher: GSA
Journal: GEOL: Geology
DOI:10.1130/G39672.1

346 Supplementary Figure 1.

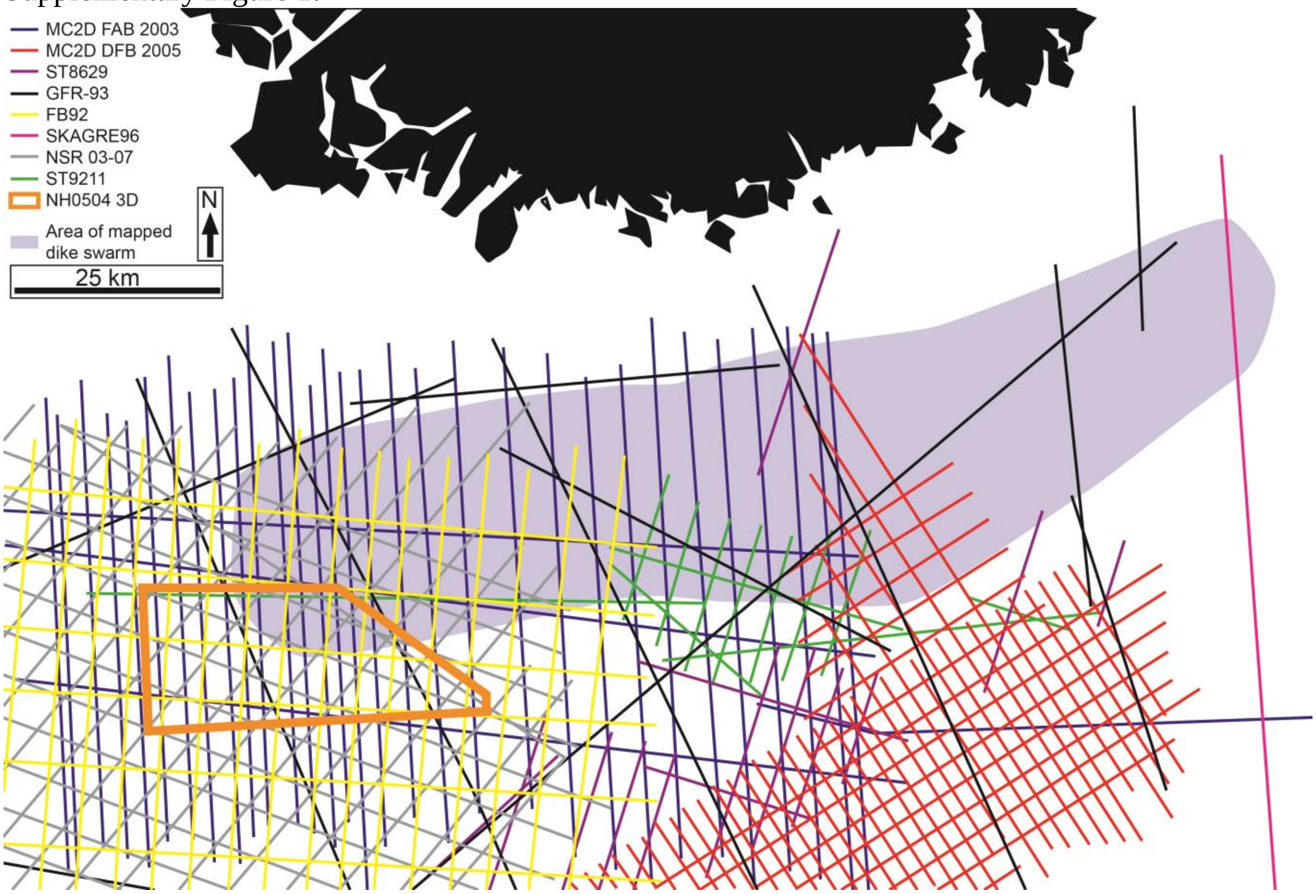

347
348
349

Publisher: GSA
Journal: GEOL: Geology
DOI:10.1130/G39672.1

Supplementary Figure 2.

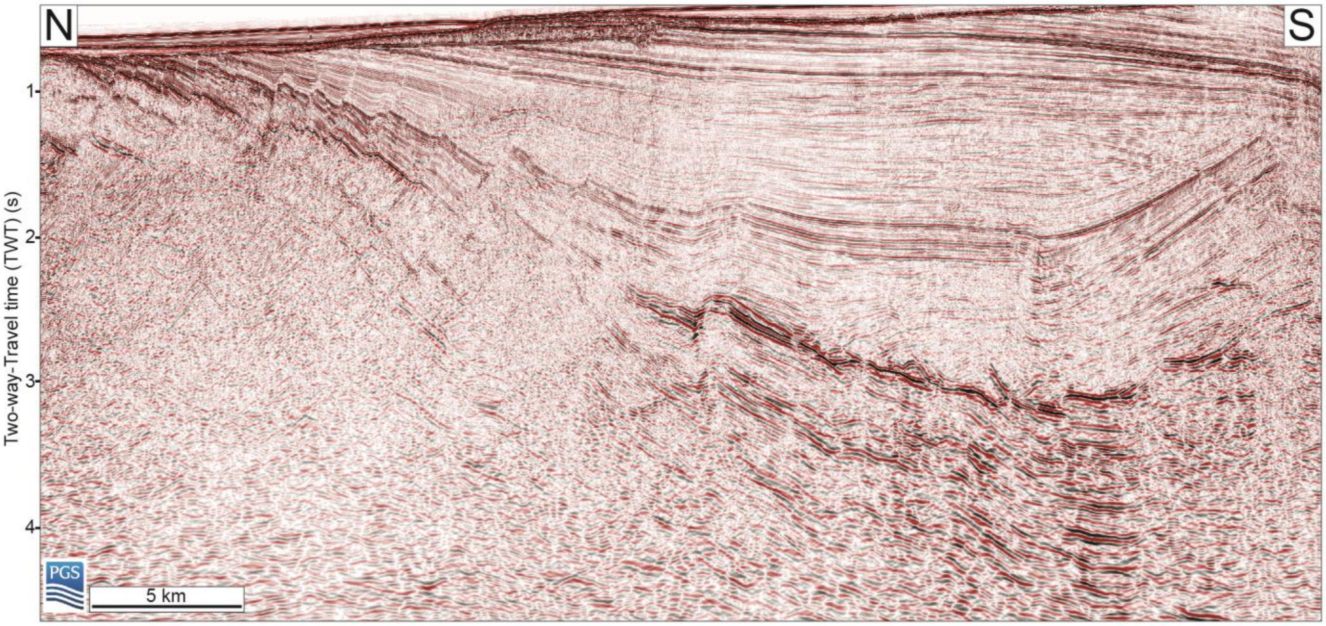

DOI:10.1130/G39672.1

Supplementary Figure 3.

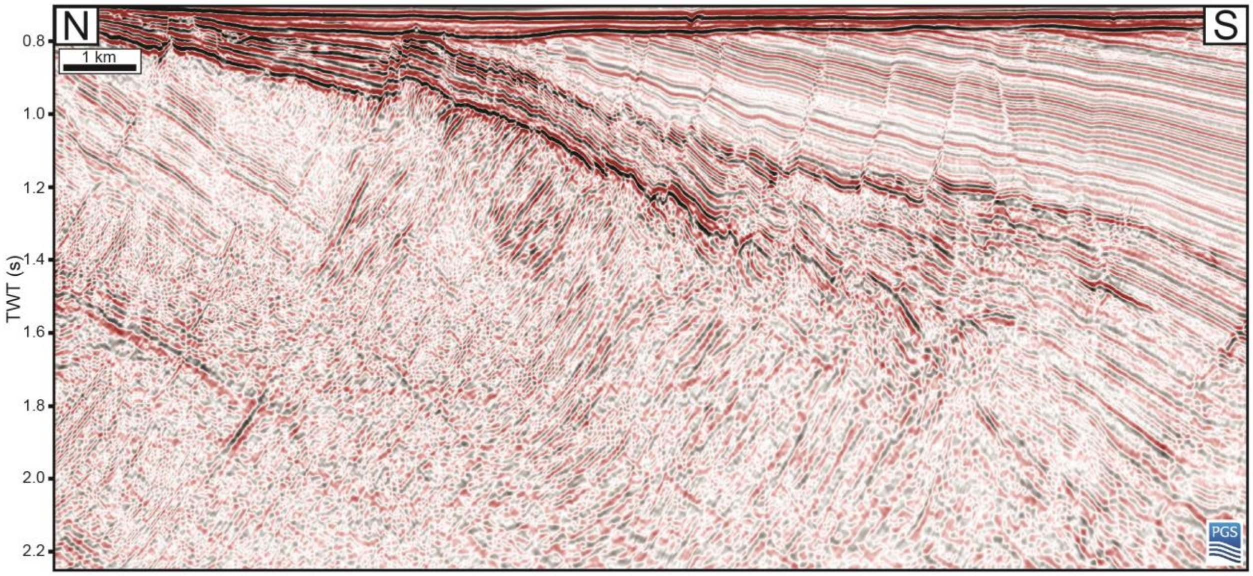

Publisher: GSA
Journal: GEOL: Geology
DOI:10.1130/G39672.1

Supplementary Figure 4

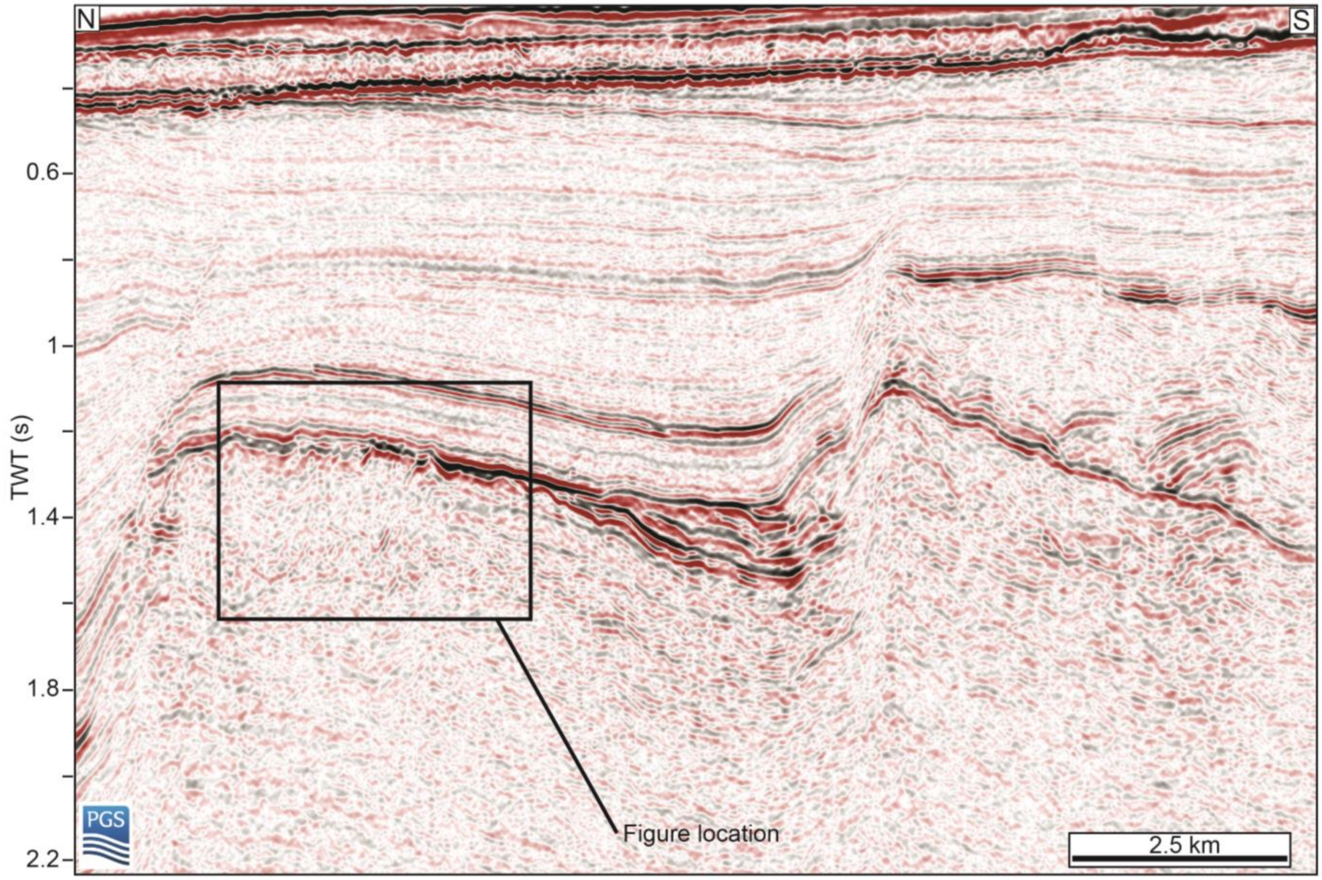

DOI:10.1130/G39672.1

Supplementary figure 5.

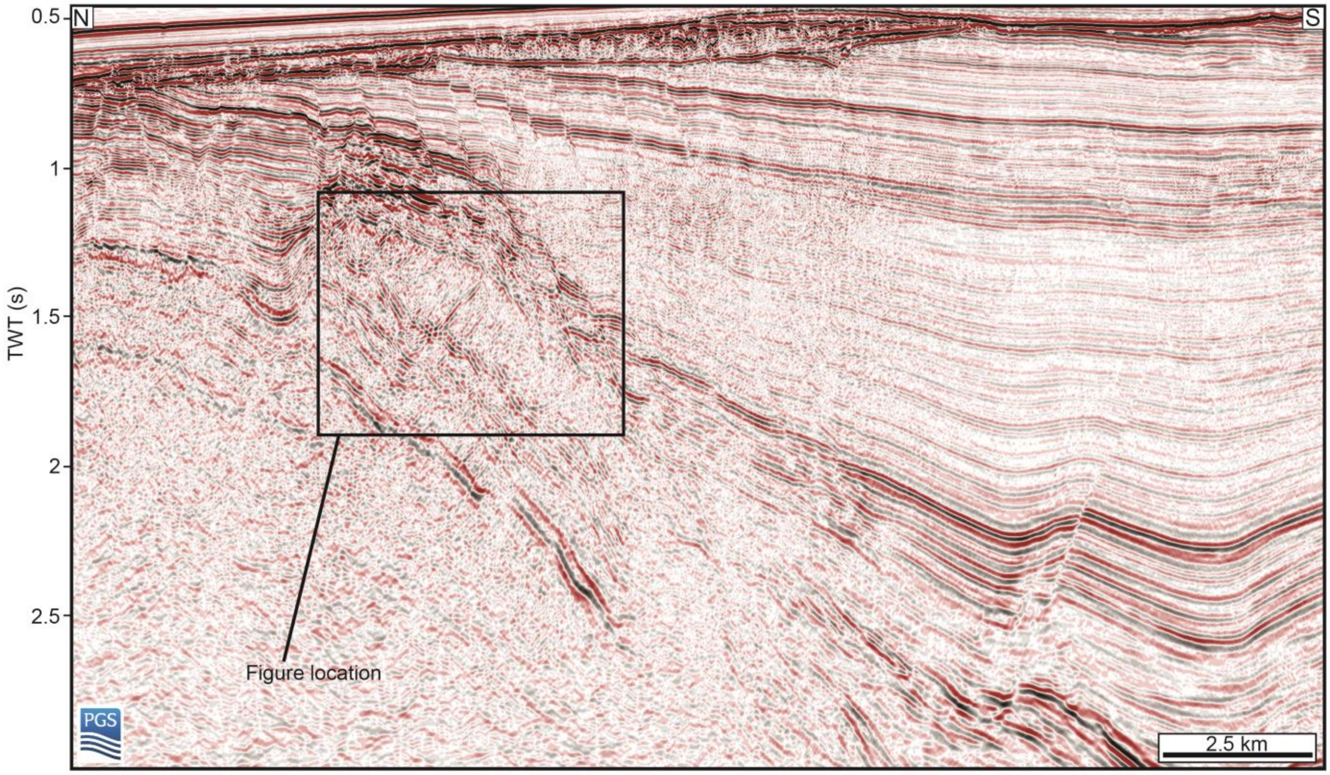

Publisher: GSA
Journal: GEOL: Geology
DOI:10.1130/G39672.1

Table S1

TABLE S1										
Dataset	Data type	Acquisition year	Record length (ms TWT)	Streamer length (m)	Fold	Shot interval (m)	Polarity (SEG convention)	Processing steps		
MC2D FAB 2003	2D	2003	7000	6000	120	25	Reverse	2D SRME	Hi-Res Radon Demultiple	Kirchoff PSTM
MC2D DFB 2005	2D	2005	8000	6000	n/a	n/a	Reverse			
ST8629	2D	1986	6000	N/A			Reverse			
GFR-93	2D	1993	12000	4500			Reverse			
FB92	2D	1992	6000	N/A			Reverse			
SKAGRE96	2D	1996	7000	3000			Reverse			
NSR03-07	2D	2003-2007	9216	8087			Reverse			
ST9211	2D	1992	7000	3000			Reverse			
NH0504	3D	2005	4040	3000			Normal			
						SRME	Surface related multiple elimination			